

A lightweight Convolutional Neural Network based on U shape structure and Attention Mechanism for Anterior Mediastinum Segmentation

Sina Soleimani-Fard¹, Won Gi Jeong², Francis Ferri Ripalda¹,

Hasti Sasani³, Younhee Choi¹, S Deiva⁴, Gong Yong Jin⁵, Seok-bum Ko¹

¹Department of Electrical and Computer Engineering, University of Saskatchewan, 57 Campus Drive, Saskatoon, SK, Canada

Email: {Vuy825, kzn518, younhee.choi, seokbum.ko}@usask.ca

²Department of Radiology, Chonnam National University Hwasun Hospital, Hwasun, South Korea

Email: wgjung86@naver.com

³Department of Electrical Engineering, Tarbiat Modares University, Al Ahmad Street, Jalal No. 7, Tehran, Iran

Email: Hastisasani@modares.ac.ir

⁴Department of Electrical Engineering, National Institute of Technology, Trichy, India.

Email: deiva@nitt.edu

⁵Department of Radiology, Research Institute of Clinical Medicine of Jeonbuk National University, Biomedical Research Institute of Jeonbuk National University Hospital, Jeonbuk National University Medical School, 20 Geonji-ro, Jeonju City, South Korea

Email: gyjin@jbnu.ac.kr

Abstract—To automatically detect Anterior Mediastinum Lesions (AMLs) in the Anterior Mediastinum (AM), the primary requirement will be an automatic segmentation model specifically designed for the AM. The prevalence of AML is extremely low, making it challenging to conduct screening research similar to lung cancer screening. Retrospectively reviewing chest CT scans over a specific period to investigate the prevalence of AML requires substantial time. Therefore, developing an Artificial Intelligence (AI) model to find location of AM helps radiologist to enhance their ability to manage workloads and improve diagnostic accuracy for AMLs. In this paper, we introduce a U-shaped structure network to segment AM. Two attention mechanisms were used for maintaining long-range dependencies and localization. In order to have the potential of Multi-Head Self-Attention (MHSA) and a lightweight network, we designed a parallel MHSA named Wide-MHSA (W-MHSA). Maintaining long-range dependencies is crucial for segmentation when we upsample feature maps. Therefore, we designed a Dilated Depth-Wise Parallel Path connection (DDWPP) for this purpose. In order to design a lightweight architecture, we introduced an expanding convolution block and combine it with the proposed W-MHSA for feature extraction in the encoder part of the proposed U-shaped network. The proposed network was trained on 2775 AM cases, which obtained an average Dice Similarity Coefficient (DSC) of 87.83%, mean Intersection over Union (IoU) of 79.16%, and Sensitivity of 89.60%. Our proposed architecture exhibited superior segmentation performance compared to the most advanced segmentation networks, such as Trans_Unet, Attention_Unet, Res_Unet, and Res_Unet++.

Index Terms—Anterior Mediastinum (AM), Self-Attention, Cross Correlation Attention, U shape structure.

*Sina Soleimani-Fard is the first author. Won Gi Jeong is the co-first author. Seok-bum Ko is the corresponding author. Gong Yong Jin is a co-corresponding author.

I. INTRODUCTION

The global utilization of Computed Tomography (CT) scans is on the rise. The UNSCEAR 2022 report estimated that globally, from 2009 to 2018, the number of examinations nearly doubled compared to 2006. Chest CT scans accounted for 12.2% of the total, making them the second most frequently performed type of CT scan, following head CTs [1]. With the increase in chest CT examinations, the detection of Anterior Mediastinal Lesions (AMLs) may also rise. Although their frequency is reported to be less than 1% [2]–[4], identifying these lesions on CT is crucial for determining subsequent management [5]. With the increase in radiological examinations, radiologist burnout has emerged as a significant issue in the medical field. One potential solution being explored is the use of Artificial Intelligence (AI) [6]. In the domain of chest radiology, the implementation of comprehensive lung cancer screening programs is anticipated to lead to an increase in the use of Low-dose Chest CT (LDCT) scans [7]. Detecting incidental AMLs on LDCT is important, as these findings may indicate the presence of tumors. This area represents a promising opportunity for radiologists to utilize AI assistance, enhancing their ability to manage workloads and improve diagnostic accuracy.

An automated segmentation model particularly tailored for the AM is a crucial prerequisite for automatically identifying AMLs in the AM, akin to lung cancer screening, which poses a significant hurdle. Retrospectively reviewing chest CT scans over a specific period to investigate the prevalence of AML requires substantial time. Additionally, the lack of

commercially available AI models makes utilizing AI for such research difficult. Developing an AI model for AML is particularly challenging because the AM does not have clear boundaries on CT scans, unlike lung parenchyma. This study establishes a hypothetical boundary for the AM and subsequently develops an AM segmentation AI model to assist in investigating the prevalence of AML.

Radiologists can now get assistance utilizing Computer-Aided Detection (CADe) techniques. By highlighting potential organ areas within CT images, CADe methods make screening more efficient and cost-effective [8] [9]. Adhering to segmentation methods is an effective strategy for successfully implementing a CADe system. Segmentation methods are useful in delineating the outlines of lesions and organs, which are essential factors for assessing the malignancy of the lesions [10]. These processes emphasize anomalies of CT imaging at the pixel level, which allows them to be distinguished from other procedures. Some methods in [11] and [12] were considered for lesion and organ segmentation, but those methods depend on handwrought features that need several manual procedures.

In recent years, Deep Neural Networks (DNN) have become a professional strategy to solve problems in many areas [13]–[15], and medical image segmentation is one of them [16], [17]. The main issues in medical image segmentation for training DNN are lack of dataset, diversity of shapes, domain shift, etc. Using pre-train models, designing lightweight and sophisticated models, and K-fold cross-validation are some methods that are used to solve issues in medical image segmentation. This work suggests a U shape architecture for segmenting the AM organ from chest CT images to aid radiologists. The proposed model identifies location of AM without any pre-processing or fine-tuning. It employs two distinct attention processes to give a rich feature map. According to the results, the proposed architecture performed better than state-of-the-art (SOTA) segmentation networks involving Res_Unet [18], Res_Unet++ [19], Trans_Unet [20], Attention_Unet [21], and Unet. The main contributions of this paper are as follows:

- This research introduced a U shape structure network for AM segmentation which uses expanded convolution and wide multi-head self-attention in the encoder. This attention effectively allows the model to learn different attention components inside separate subspaces and long range dependencies.
- Specifically, we used Channel Depth-Wise Cross-Correlation Attention (CD-WCC) in the encoder to find similarities between the encoder and decoder to improve organ localization.
- The proposed architecture is more lightweight than the SOTA network, with just 6.7 million parameters while it has achieved acceptable and higher performance in all metrics.
- To show that our proposed architecture is not limited to our proposed encoder, we used Resnet18 [22] and the encoder part of the original Unet as the encoder part in the proposed network. These results illustrates the

effectiveness of the proposed structure.

The rest of the paper is organized as follows: Section II provides a summary of the related research on image segmentation using the Unet framework. In Section III, we elaborate each details of the proposed Unet. Next, Section IV describes an overview of datasets and the methodologies used to analyze and validate the accuracy of AM segmentation and experimental results. In Section V, we show the advantage of the proposed network compared to SOTA networks. Finally, the conclusions can be found in Section VI.

II. RELATED WORKS

Unet [23] structure was one of the first DNN networks introduced for segmentation. Many researchers have proposed their segmentation network based on Unet. ViT was proposed for image recognition by Dosovitskiy et al. [24]. Inspired by ViT, Chen et al. [20] introduced Trans_Unet, which combined transformer and CNN for the encoder part of their proposed Unet. Trans_NUnet [25], by maintaining the structure of Trans_Unet in the encoder and using the Convolutional Block Attention Module (CBAM) [26] in the decoder improved performance in Dice score. In [27], fine spatial information was recovered by utilizing Multi-Head Cross-Attention (MHCA) in the decoder. The transformer block is always used in the encoder part to find long-range dependencies, while Petit et al. [27] implemented the transformer in the decoder to introduce the U-Transformer.

Xu et al. [28] utilized LeViT [29], which has four convolution blocks for the encoder part, to propose LeViT Unet. This was the first segmentation work in medical imaging to use transformer architecture to enhance speed. Additionally, they paid attention to potential information by adding attention bias to the attention MLP block. By replacing traditional convolution layer in Unet by transformer introduced UNETR [30]. In their work, transformer extracted features map. Shaker et al. introduced UNETR++ in [31] by focusing on channel and spatial attention. Their main idea was an Efficient Paired Attention (EPA) block. While drastically lowering network complexity, UNETR++ outperformed UNETR. Swin UNERT [32] used Swin transformer [33] for the feature extractor in the encoder part. Based on the Swin transformer’s shifting window, their model can learn multi-scale contextual and capture long-range dependencies, outperforming ViT.

Res_Unet [18] is a development of the Unet structure, which uses residual connections for the decoder and encoder. In addition, to improve performance, they used an atrous convolution block, multi-tasking inference, and pyramid pooling. Deep residual networks in Resnet architecture and Unet structure were used to design Res_Unet++ [19]. The residual block facilitates the transmission of information between layers, enabling the construction of a more profound neural network capable of addressing each encoder’s degradation issue. This enhances the interconnections between channels, thereby decreasing the computational expenditure. The Res_Unet++ design consists of a stem block, three encoder blocks, an

Atrous Spatial Pyramid Pooling (ASPP) module, and three decoder blocks.

Attention methods have been developed to enhance the performance of DNNs by enabling them to concentrate on the most significant aspects of the input. However, based on the input feature map, Multi-Head Self-Attention (MHSA) can be a heavyweight network. Traditional MHSA in transformers are the main reason Trans_Unet is heavyweight. U-Transformer used one MHSA, which has 5 million parameters. Our proposed network takes a more efficient approach to utilizing MHSA. Instead of using one MHSA, we leverage the advantage of parallel MHSA. By splitting the input feature map into smaller chunks and utilizing parallel MHSA, we significantly reduce the number of parameter in the proposed network.

III. PROPOSED NETWORK ARCHITECTURE

The proposed architecture shown in Fig. 1 was designed in U shape structure which has three components: encoder, decoder, and parallel path connection between encoder and decoder. The encoder extracts feature maps and decreases input dimensions from $3 \times 224 \times 224$ to $512 \times 7 \times 7$. The decoder improves feature maps' dimensions relative to the input dimension size. Both the encoder and decoder are designed into five sequential stages. Moreover, we employ two highly effective attention methods to significantly bolster the restoration of organ segmentation in each decoder and encoder block, instilling confidence in the model's capabilities. After improving height and width in decoder, channel attention applies to channels dimension. Instead of using average and maximum in height and width for channel attention, we utilize depth-wise cross correlation [34] in order to find similarity feature maps between each stage in encoder and decoder. In the next step, the effective of similarity multiply to feature maps. Parallel path connection is designed into five dilated convolutions with different filter size and dilation rate. Dilated convolutions provide advantages such as enhanced receptive field size and retrieving features at several scales.

A. Expanding Convolution block

Going wider into the feature extraction section, we expand the convolutional layer and build the proposed feature extraction in five stages which is illustrated in Fig. 2. In addition, 1×1 convolutions are employed as opposed to 3×3 convolutions as main part of extract features. The input channel for every step is separated into smaller chunks, and then a separate convolution filter is applied independently for each smaller channel. In order to be ready for the next stage, the specific features from all channels are concatenated in channel dimension and then pass through one 3×3 convolutional layer. The input image size is $3 \times 224 \times 224$.

- In stage 0, according to the input channel, three different 1×1 convolution layers are applied independently. After concatenation, one 3×3 convolution layer improves channel to 64 while height and width decrease to 112.

- In stage 1, 64 channels are divided into 2. Two $32 \times 112 \times 112$ passes through the 1×1 convolution layers simultaneously and are concatenated in the channel dimension to return to 64 channels then resulting in a feature extractor size will be $128 \times 56 \times 56$.
- The exact structure, like stage 1, is considered for stage 2. However, the output size's channel, height, and width dimensions will be 128, 28, and 28, respectively.
- Stage 3 is designed to be deeper and broader than other stages to capture more complicated features and patterns as the input data progresses through the network. Although it maintains the same structure as previous stages, it involves four 1×1 convolutions simultaneously, concatenation, and one additional 3×3 convolution. Finally, the feature extraction from stage 3 results in a size of $256 \times 14 \times 14$.
- The strategy for designing stage 4 is the same as the previous stage. However, the input channel size is 256, divided by 2. Therefore, two $64 \times 14 \times 14$ enter to two 1×1 convolutions independently. The output size will be $512 \times 7 \times 7$ after concatenation, passing from one 3×3 convolution.

B. Wide Multi-Head Self-Attention (W-MHSA)

The attention mechanism can be heavy weight according to the input dimension because due to fully connected layer. In this study, height and width of feature maps is divided into small chunks to overcome the heavy weight of self-attention. Three different MHSA are utilized in encoder of the proposed network. Four parallel MHSA shown in (Fig. 3(a)), two parallel MHSA shown in (Fig. 3(b)), and one MHSA shown in (Fig. 3(c)) are used in stages 1 and 2, stage 3, and stage 4, respectively. Parallel MHSA are named Wide-MHSA (W-MHSA) in this study.

- After passing the input from stage 1, the output will be $64 \times 56 \times 56$. First, W-MHSA (rate of width = 4) is applied after stage 1. W-MHSA (rate of width = 4) is designed in four branches. Therefore, the input for W-MHSA (rate of width = 4) is divided into 4 in height and width. First, four $64 \times 14 \times 14$ enter to four different MHSA. Second, four outputs from MHSA are concatenated in height and width dimensions. These outputs from concatenations are again concatenated by height and weight, and then two concatenation phases multiply together. Finally, it passes from one convolution layer.
- Furthermore, there is a comparable procedure for stage 2. The input $128 \times 28 \times 28$ is split by 4. Subsequently, four $128 \times 7 \times 7$ enter four separate MHSA using a methodology similar to stage 1.
- After stage 3 is completed, the input size is $256 \times 14 \times 14$. The steps are the same as in the previous phases, with the exception that the width and height are split in two. $2 \times (256 \times 7 \times 7)$ is passed from each of the two parallel MHSA employed (W-MHSA(rate of width = 2)). Height and width are concatenated from two MHSA outputs

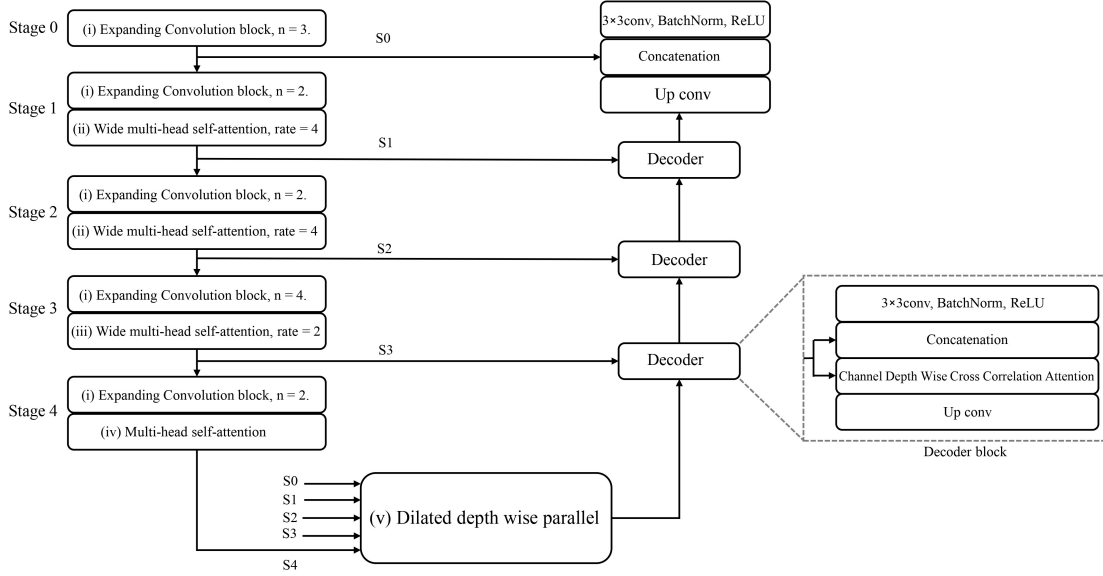


Fig. 1: Proposed network for anterior mediastinum segmentation. (i): Expanding convolution block introduced in Fig. 2, n refers to amount of 1×1 based on input feature map. (ii): Fig. 3 (a) is related to four parallel MHSA used for the proposed network. (iii): W-MHSA with rate 2 is utilized two MHSA in the parallel way shown in Fig. 3 (b). (iv): Traditional MHSA shown in Fig. 3 (c). (v): Delited depth-wise parallel shown in Fig. 5.

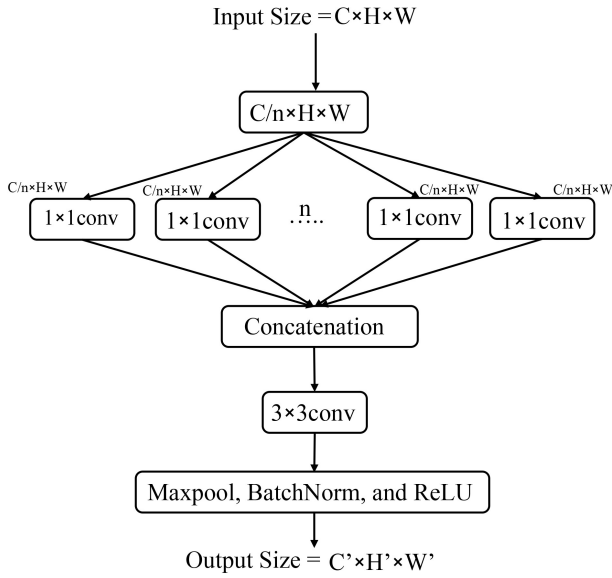


Fig. 2: Expanding convolution block (shown in Fig. 1). The feature map channel is divided into small chunks according to the number of n for each stage: stage 0 = 3, stage 1 = 2, stage 2 = 2, stage 3 = 4, stage 4 = 2.

in height and width dimension. Then, these two concatenations are concatenated again regarding height and width dimensions. Finally, the last two concatenations are multiplied and passed to a convolution layer.

- In addition, one MHSA is used for after stage 4 which the input dimension is $512 \times 7 \times 7$. We provide more details of W-MHSA in Fig. 3, in which (a) divides input size to 4, (b) divides to 2, and (c) is the original MHSA.

C. Channel Depth Wise Cross Correlation Attention (CDWCC)

The cross-correlation module is a computational process that convolves two sets of feature maps. It is typically employed for tracking purposes in techniques like SiamRPN++ [34]. The mechanism of working in this module is similar to that of two distinctive feature maps. This study uses cross-correlation to find similarities between the encoder and decoder. The correlation procedure is performed channel by channel on the two different feature maps with an equal number of channels, height, and width. According to Fig. 4, the decoders' features map is input for CDWCC, while the encoders' features map is a kernel for performing the correlation operation channel by channel to find similarity. Finally, the CDWCC feature map is multiplied element-wise with the decoder feature map.

D. Dilated depth wise parallel path connection (DDWPP)

In order to have high field of view, DDWPP is designed. As shown in Fig. 5, it has five parallel dilated convolutions with different kernel size and dilated rate which capture large receptive fields without increasing the number of parameters. In the process of segmentation, down sampling feature maps can potentially discard crucial components. Therefore, preserving information from the initial stages of the encoder is imperative

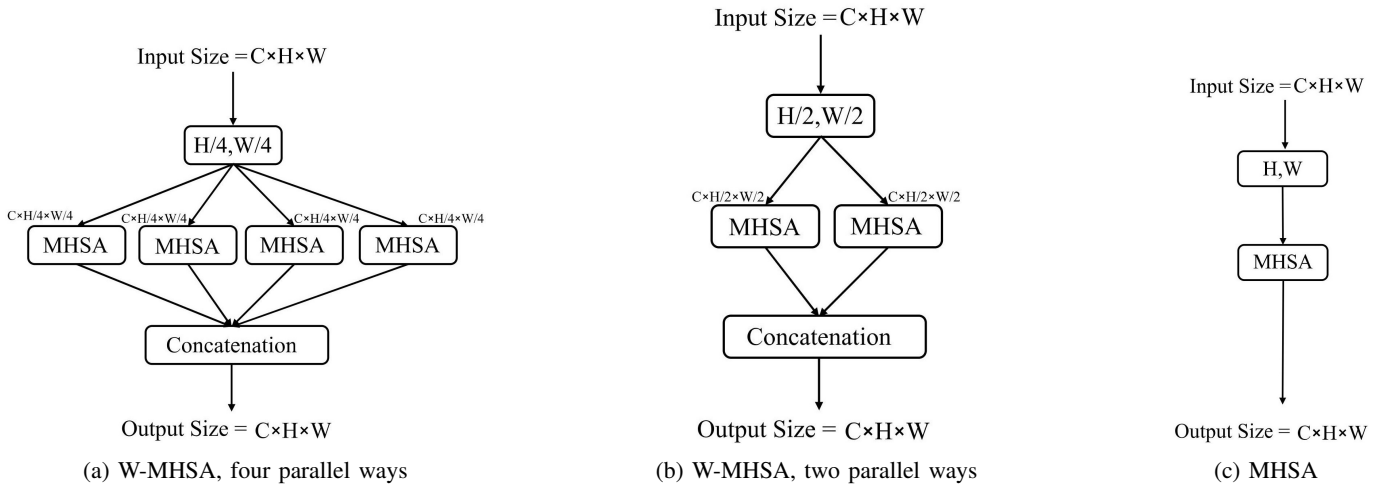


Fig. 3: Attention with different parallel paths. (a): It is designed with four MHSA (rate of width = 4) (shown in (ii) in Fig. 1), (b): It is designed with two MHSA (rate of width = 2) (shown in (iii) in Fig. 1), and (c): It is designed with one MHSA (shown in (iv) in Fig. 1).

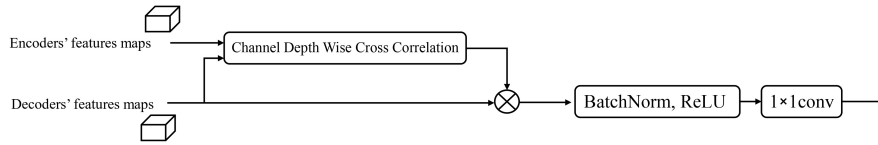


Fig. 4: Channel Depth Wise Cross Correlation Attention (shown in decoder part of Fig. 1)

for the subsequent up sampling phase. Having feature maps of each stage effectively helps our proposed network avoid missing information. In addition, primary stages have low level information while the latest stages have valuable one. As seen in Fig. 5, the dilated convolution technique expands the receptive field while maintaining the spatial precision of the feature maps. We have used four parallel dilated convolutions in the DDWPP block to increase the detection sensitivity for small AMs. The four dilated convolutions follow dilated rates of 16, 8, 4, and 2, and filter sizes of 7×7 , 5×5 , 5×5 , and 3×3 , respectively.

IV. MATERIALS AND EXPERIMENTS

This study was approved by the Institutional Review Board of Chonnam National University Hwasun Hospital (CNUHH-2022-241). Informed consent was waived due to its retrospective design.

A. Dataset

This study was conducted with 200 patients who underwent chest CT as part of a health check-up at CNUHH between September 2020 and December 2021, and who exhibited no AMLs in the anterior mediastinum. A thoracic radiologist with 5-years of experience in chest radiology (W.G.J.) visually reviewed all chest CT scans and selected those without AMLs. The mean age of the patients was 55.9 years (SD, 10.0 years), and the cohort comprised 120 males (60%) and 80 females (40%). We defined anterior mediastinum as following criteria:

(i) superior border: thoracic inlet, (ii) Inferior border: base of pulmonary trunk, (iii) anterior border: posterior margin of sternum, (iv) posterior border: anterior aspect of pericardium, and (v) lateral border: parietal mediastinal pleura [2]. Detailed CT parameters are described in the Table ??.

2776 slices from 200 patients were considered for training the Deep Learning (DL) model. Initially, we transformed Digital Imaging and Communications in Medicine (DICOM) into PNG format, a technological standard for digitally storing and transmitting medical images. We considered the traditional mediastinal window settings, which included a window level of 30 and a window width of 520 Hounsfield Units (HU). Finally, the generated PNG images had resolutions of 512×512 , and a radiologist manually drew masks for AM using the labelme [35] annotation tool. As shown in Fig. 6, an AM present in two slice images has distinct visual depictions with resolutions of 512×512 , HU of 520, and window level of 30.

B. Evaluation metrics

Our study utilizes Dice Similarity Coefficient (DSC), mean Intersection over Union (IoU), sensitivity, and Accuracy (Acc), to comprehensively examine and evaluate the effectiveness of our SOTA research technique. The equations representing DCS, IoU, sensitivity, and Acc are expressed as equations (1), (2), (3), and (4) accordingly. The metrics are computed based on the values of True Positive (TP), False Positive (FP), True Negative (TN), and False Negative (FN). TP and TN represent the accuracy of positive and negative predictions, respectively.

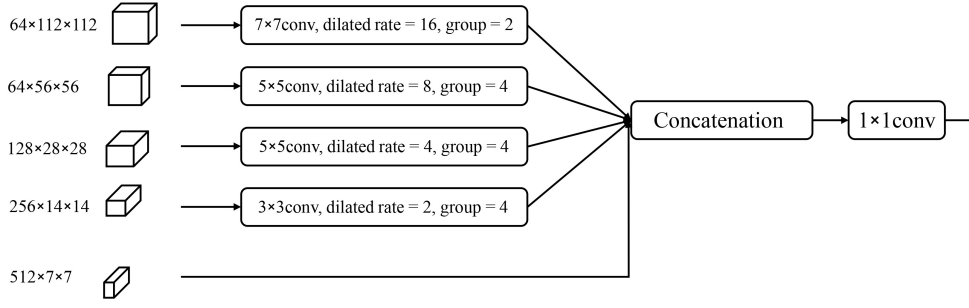


Fig. 5: Dilated depth wise parallel path connection (shown in (v) in Fig. 1). The input channels are convolved separately with their own sets of filters, each based on a distinct number of groups.

TABLE I: Detailed CT parameters

CT machine (Vendor)	Parameters
Revolution HD (GE Healthcare, Waukesha, WI, USA)	Section thickness: 2.5–5.0 mm Rotation time: 0.5 s Peak kilovoltage: 120 kVp Tube current: 60–220 mAs, with an automatic exposure control Kernel: standard Reconstruction algorithm: iterative reconstruction
Somatom Definition Flash (Siemens Healthineers, Erlangen, Germany)	Section thickness: 3.0–4.0 mm Rotation time: 0.5 s Peak kilovoltage: 100 kVp, 120 kVp Tube current: 60–220 mAs, with an automatic exposure control Kernel: B31f Reconstruction algorithm: iterative reconstruction

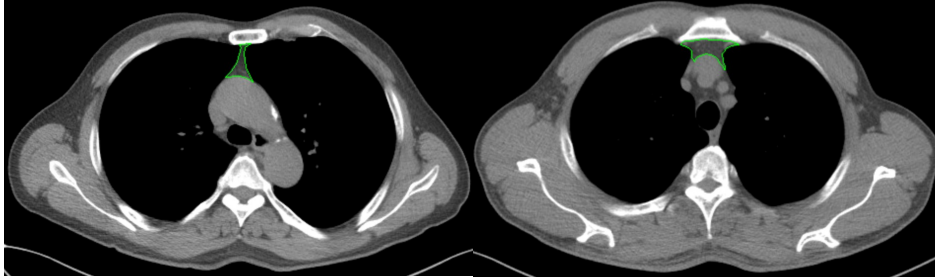


Fig. 6: Two distinct anterior mediastinal instances from one patient are shown inside the green border to illustrate diverse shape of AM.

FP and FN indicate the ratio of positive predictions that were wrongly forecasted and negative predictions that were incorrectly predicted, respectively.

$$Dice = \frac{2TP}{2TP + FP + FN} \quad (1)$$

$$IoU = \frac{TP}{TP + FP + FN} \quad (2)$$

$$Sensitivity = \frac{TP}{TP + FN} \quad (3)$$

$$Accuracy = \frac{TN + TP}{TN + TP + FN + FP} \quad (4)$$

C. Implementation details

For both the training and validation phases, we used 4-fold cross-validation, with each model being trained using 100 epochs per fold. The loss function used is dice loss [36], in which loss is optimized by utilizing Adam with an initial learning rate of 0.0003. The learning rate was decreased by 10 times in epochs 25 and 180. In addition, 32 batch sizes were considered. Pytorch framework was used to implement the proposed and other networks on A40 GPU.

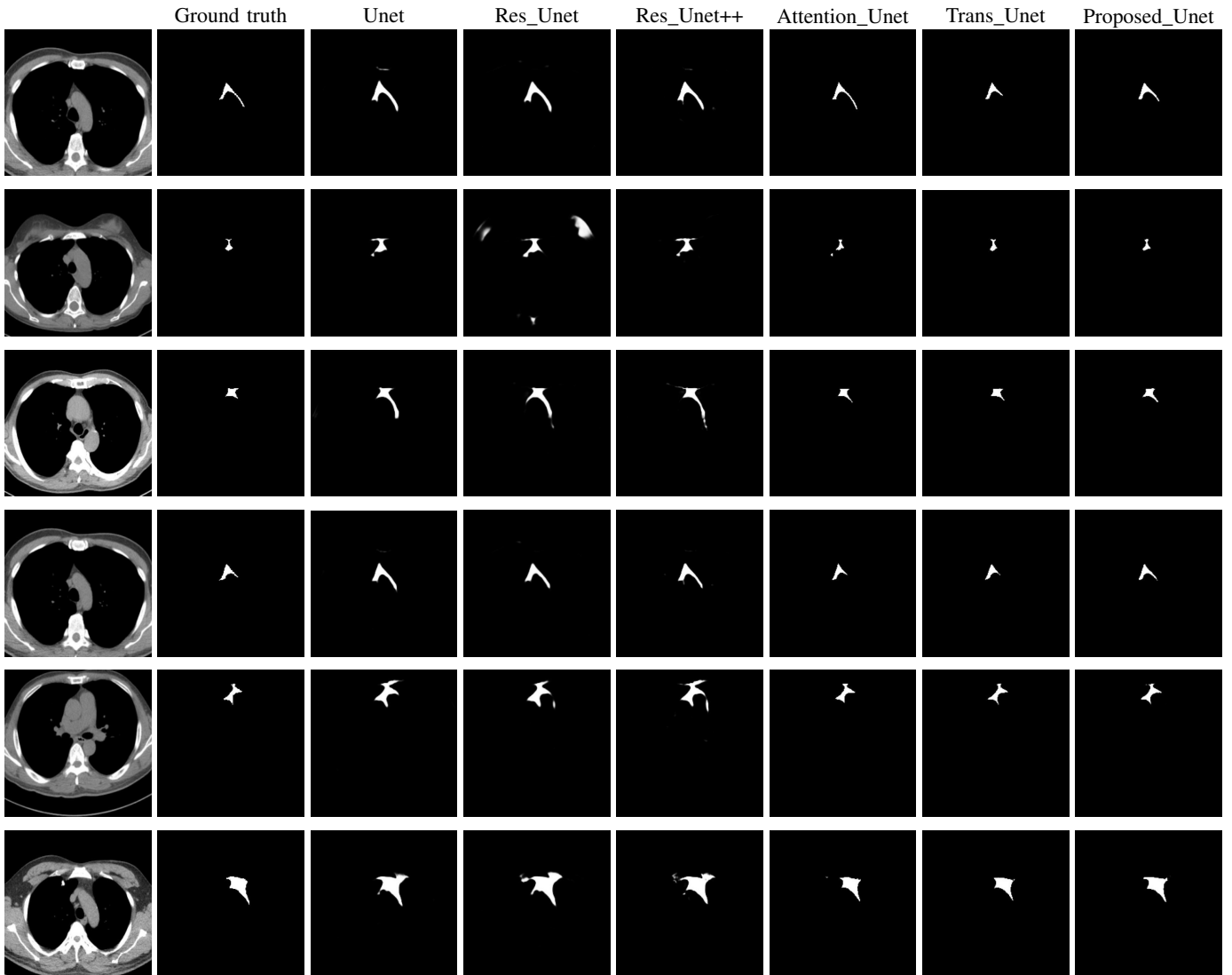


Fig. 7: Visual comparison of distinct models.

V. EVALUATION

In this section, we first compared the proposed method to the SOTA network. Then, in the subsection on the proposed method’s effectiveness, we used different feature extractions, such as Resnet18 and the encoder part of the original Unet, to show the flexibility of our proposed architecture in using various feature extractions in the encoder part. These results showed that with almost the same structure in the encoder of Unet, Res_Unet, and Res_Unet++, the proposed method with different feature extraction performed better than those.

A. Result

Table II outlines the segmentation results of SOTA networks and our proposed model. As shown, because of various shapes of AM, just complicated network achieved acceptable results. Res_Unet++ and Res_Unet are two networks demonstrated inferior performance for all metrics. DCS, IoU, sensitivity, and Acc were obtained at 55.95%, 39.93%, 39.97%, and

98.83%, respectively, for Res_Unet. Res_Unet++ is the development of Res_Unet, which performs better than Res_Unet. All metrics were as follows: DSC = 59.80%, IoU = 43.83, sensitivity = 43.92%, and Acc 99.09%.

Trans_Unet is another SOTA network that was considered for comparison. Based on the transformer modules as encoder part of this network, all results were higher than Res_Unet and Res_Unet++. DCS, IoU, sensitivity, and ACC were achieved at 85.50%, 75.98%, 85.32%, and 99.80, respectively, for Trans_Unet. Attention_Unet obtained 86.99% in DSC, 78.28% in IoU, 87.36% in sensitivity, and 99.84% Acc. Compared to all network, our proposed network performed better in DSC (87.69%), IoU (78.81%), and sensitivity (87.69%) while it has significantly less parameters (6.7 M).

Fig. 7 shows the comparative analysis of several networks on our AM dataset. When the AM structures of interest have a small visual form, Trans_Unet and the proposed network

performed better in AM segmentation (second row of Fig. 7). The findings demonstrate the MHSA enhances the network’s capacity to capture more contextual information, enabling it to distinguish the AM organ from the surrounding organs. The results demonstrate the effectiveness of the MHSA in AM segmentation. Networks such as Unet, Res_Unet, and Res_Unet++, which do not utilize MHSA, struggle to segment AM. In contrast, attention_Unet, Trans_Unet, and the proposed, which incorporate attention, outperform the former.

B. Effectiveness of proposed backbone

In Table III, we illustrated the effectiveness of the proposed Unet backbone by using Resnet18 and the encoder part of the original Unet. Proposed Unet (encoder = Resnet18) showed approximately 30% higher performance in each metric while having higher parameters (15.2 M vs. 13.05 M and 14.48 M) than Res_Unet and Res_Unet++. The results of the proposed network illustrate that each metrics (DSC = 86.91%, IoU = 77.75%, sensitivity = 87.62%, and Acc = 99.83%) has competitive value compared to Attention_Unet. In addition, a Consecutive Convolution Block (CCB)-based encoder of original Unet was designed. We used the same structure for the original Unet by adding normalization layers to be robust and efficient. As shown in Fig. 8 (a), this convolution layer involves one 3×3 convolution, normalization layer and activation function, which are repeated twice. As shown in Fig. 8 (b), encoder of Unet was designed in five stages with 64, 64, 128, 256, and 512 channels. Results of the proposed network (encoder = consecutive convolution block) demonstrated that our proposed structure is not limited to our proposed encoder. It showed DSC = 87.70%, IoU = 78.83%, sensitivity = 87.85%, and Acc = 99.80%, which is the second-best value behind the initially proposed network as shown Table III.

The results of this section demonstrates the effectiveness of the proposed DDWPP and CDWCC.

VI. CONCLUSION

To automatically detect Anterior Mediastinum (AM) in the Computed Comography (CT) scans, we proposed an architecture based on the U-shaped structure. For our proposed network, an expanded convolution block and W-Multi-Head Self-Attention (W-MHSA) were utilized as feature extraction. Channel Depth Wise Cross Correlation Attention (CDWCC) was introduced in decoder of the proposed network to find similarities in feature maps from the encoder and decoder. In addition, Dilated Depth-Wise Parallel Path connection (DDWPP) has been proposed as connection between encoder and decoder of the proposed U-shaped network in order to maintain long range dependencies. A dataset of 200 AM patients was used to justify the effectiveness of the proposed network. According to the results, the proposed network obtained 87.83% in DSC, 79.16% in IoU, and 89.60% in Sensitivity, which are higher than those of SOTA networks, while it has significantly fewer parameters (6.7 M).

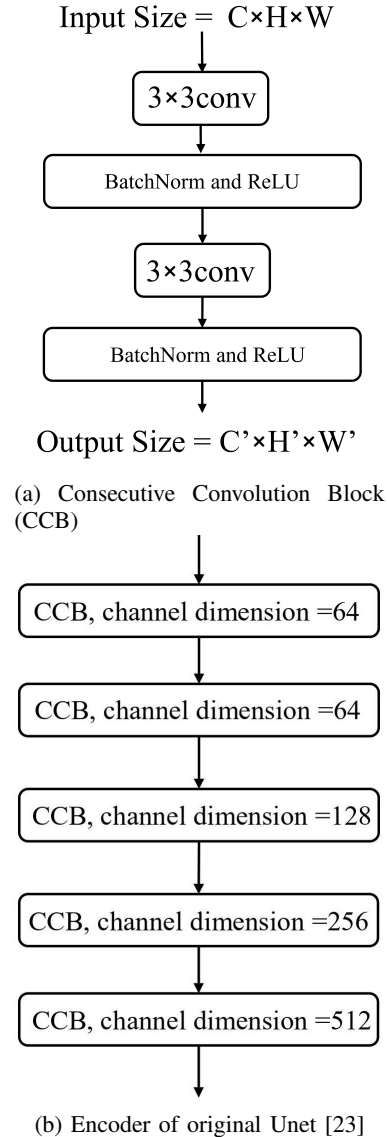


Fig. 8: (a) : Consecutive Convolution Block (CCB). The original block used in Unet [23] was designed without normalization layers. However, in this study we added batchnorm in to CCB. (b): We used this structure in Fig. 1 as feature extractor.

For future work, we anticipate the following clinical utilities for the proposed model for the automatic segmentation of AM in this study: (i) automatic detection and classification of AML in chest CT, including LDCT; (ii) distribution analysis of anterior mediastinal volume according to clinical factors such as age and sex; and (iii) educational purposes for medical students, healthcare professionals, and the general public.

TABLE II: Results of AM segmentation for different methods

Model	DCS (%)	IoU (%)	Sensitivity (%)	Acc (%)	Parameters (M)
Trans_Unet	85.50	75.98	85.32	99.80	88
Attention_Unet	86.99	78.28	87.36	99.84	34.87
Unet	63.04	47.05	47.11	98.21	31.03
Res_Unet	55.95	39.93	39.97	98.93	13.05
Res_Unet++	59.80	43.83	43.92	99.09	14.48
Proposed network	87.83	79.16	89.60	99.83	6.7

TABLE III: Results of effectiveness the proposed backbone with different encoder.

Model (Proposed_Unet)	DCS (%)	IoU (%)	Sensitivity (%)	Acc (%)	Parameters (M)
Encoder: Expanding Convolution block	87.83	79.16	89.60	99.83	6.7
Encoder: Resnet18	86.91	77.75	87.62	99.83	15.2
Encoder: Consecutive convolution block	87.70	78.83	87.85	99.80	8.8

REFERENCES

- [1] U. N. S. C. on the Effects of Atomic Radiation, *Sources, Effects, and Risks of Ionizing Radiation. Evaluation of Medical Exposure to Ionizing Radiation. Vol 1, Scientific Annex A. 2020/2021 Report to the General Assembly with Annexes.* New York, NY: United Nations, 2022.
- [2] S. H. Yoon, S. H. Choi, C. H. Kang, and J. M. Goo, "Incidental anterior mediastinal nodular lesions on chest ct in asymptomatic subjects," *Journal of Thoracic Oncology*, vol. 13, no. 3, pp. 359–366, 2018.
- [3] C. I. Henschke, I.-J. Lee, N. Wu, A. Farooqi, A. Khan, D. Yankelevitz, and N. K. Altorki, "Ct screening for lung cancer: prevalence and incidence of mediastinal masses," *Radiology*, vol. 239, no. 2, pp. 586–590, 2006.
- [4] T. Araki, M. Nishino, W. Gao, J. Dupuis, G. R. Washko, G. M. Hunninghake, T. Murakami, G. T. O'Connor, and H. Hatabu, "Anterior mediastinal masses in the framingham heart study: prevalence and ct image characteristics," *European journal of radiology open*, vol. 2, pp. 26–31, 2015.
- [5] R. F. Munden, B. W. Carter, C. Chiles, H. MacMahon, W. C. Black, J. P. Ko, H. P. McAdams, S. E. Rossi, A. N. Leung, P. M. Boiselle *et al.*, "Managing incidental findings on thoracic ct: mediastinal and cardiovascular findings. a white paper of the acr incidental findings committee," *Journal of the American College of Radiology*, vol. 15, no. 8, pp. 1087–1096, 2018.
- [6] C. R. Bailey, A. M. Bailey, A. S. McKenney, and C. R. Weiss, "Understanding and appreciating burnout in radiologists," pp. E137–E139, 2022.
- [7] A. Wolf, K. C. Oeffinger, T. Y.-C. Shih, L. C. Walter, T. R. Church, E. T. Fontham, E. B. Elkin, R. D. Etzioni, C. E. Guerra, R. B. Perkins *et al.*, "Screening for lung cancer: 2023 guideline update from the american cancer society," *CA: A Cancer Journal for Clinicians*, 2023.
- [8] H. R. Roth, L. Lu, J. Liu, J. Yao, A. Seff, K. Cherry, L. Kim, and R. M. Summers, "Improving computer-aided detection using convolutional neural networks and random view aggregation," *IEEE transactions on medical imaging*, vol. 35, no. 5, pp. 1170–1181, 2015.
- [9] R. Castro-Zunti, E. H. Park, Y. Choi, G. Y. Jin, and S.-b. Ko, "Early detection of ankylosing spondylitis using texture features and statistical machine learning, and deep learning, with some patient age analysis," *Computerized Medical Imaging and Graphics*, vol. 82, p. 101718, 2020.
- [10] W. Jung, S. Cho, S. Yum, Y. K. Lee, K. Kim, and S. Jheon, "Differentiating thymoma from thymic cyst in anterior mediastinal abnormalities smaller than 3 cm," *Journal of Thoracic Disease*, vol. 12, no. 4, p. 1357, 2020.
- [11] T. Sandor, D. Metcalf, and Y.-J. Kim, "Segmentation of brain ct images using the concept of region growing," *International journal of biomedical computing*, vol. 29, no. 2, pp. 133–147, 1991.
- [12] X. Ye, G. Beddoe, and G. Slabaugh, "Automatic graph cut segmentation of lesions in ct using mean shift superpixels," *Journal of Biomedical Imaging*, vol. 2010, pp. 1–14, 2010.
- [13] S. S. Fard, M. Kaveh, M. R. Mosavi, and S.-B. Ko, "An efficient modeling attack for breaking the security of xor-arbiter puffs by using the fully connected and long-short term memory," *Microprocessors and Microsystems*, vol. 94, p. 104667, 2022.
- [14] J. Torres-Tello, A. V. Guaman, and S.-B. Ko, "Improving the detection of explosives in a mox chemical sensors array with lstm networks," *IEEE Sensors Journal*, vol. 20, no. 23, pp. 14 302–14 309, 2020.
- [15] S. S. Fard, A. Amirkhani, and M. Mosavi, "Retinamhsa: Improving in single-stage detector with self-attention," in *2021 7th International Conference on Signal Processing and Intelligent Systems (ICSPIS)*. IEEE, 2021, pp. 1–5.
- [16] Y. Wang, W. G. Jeong, H. Zhang, Y. Choi, G. Y. Jin, and S.-B. Ko, "Anterior mediastinal nodular lesion segmentation from chest computed tomography imaging using unet based neural network with attention mechanisms," *Multimedia Tools and Applications*, pp. 1–19, 2023.
- [17] K. J. Chae, G. Y. Jin, S. B. Ko, Y. Wang, H. Zhang, E. J. Choi, and H. Choi, "Deep learning for the classification of small (2 cm) pulmonary nodules on ct imaging: a preliminary study," *Academic radiology*, vol. 27, no. 4, pp. e55–e63, 2020.
- [18] F. I. Diakogiannis, F. Waldner, P. Caccetta, and C. Wu, "Resunet-a: A deep learning framework for semantic segmentation of remotely sensed data," *ISPRS Journal of Photogrammetry and Remote Sensing*, vol. 162, pp. 94–114, 2020.
- [19] D. Jha, P. H. Smedsrud, M. A. Riegler, D. Johansen, T. De Lange, P. Halvorsen, and H. D. Johansen, "Resunet++: An advanced architecture for medical image segmentation," in *2019 IEEE international symposium on multimedia (ISM)*. IEEE, 2019, pp. 225–2255.
- [20] J. Chen, Y. Lu, Q. Yu, X. Luo, E. Adeli, Y. Wang, L. Lu, A. L. Yuille, and Y. Zhou, "Transunet: Transformers make strong encoders for medical image segmentation," *arXiv preprint arXiv:2102.04306*, 2021.
- [21] O. Oktay, J. Schlemper, L. L. Folgoc, M. Lee, M. Heinrich, K. Misawa, K. Mori, S. McDonagh, N. Y. Hammerla, B. Kainz *et al.*, "Attention u-net: Learning where to look for the pancreas," *arXiv preprint arXiv:1804.03999*, 2018.
- [22] K. He, X. Zhang, S. Ren, and J. Sun, "Deep residual learning for image recognition," in *Proceedings of the IEEE conference on computer vision and pattern recognition*, 2016, pp. 770–778.
- [23] O. Ronneberger, P. Fischer, and T. Brox, "U-net: Convolutional networks for biomedical image segmentation," in *Medical image computing and computer-assisted intervention—MICCAI 2015: 18th international conference, Munich, Germany, October 5–9, 2015, proceedings, part III 18*. Springer, 2015, pp. 234–241.
- [24] A. Dosovitskiy, L. Beyer, A. Kolesnikov, D. Weissenborn, X. Zhai, T. Unterthiner, M. Dehghani, M. Minderer, G. Heigold, S. Gelly *et al.*, "An image is worth 16x16 words: Transformers for image recognition at scale," *arXiv preprint arXiv:2010.11929*, 2020.
- [25] X. Yang and X. Tian, "Transunet: Using attention mechanism for whole heart segmentation," in *2022 IEEE 2nd International Conference on Power, Electronics and Computer Applications (ICPECA)*. IEEE, 2022, pp. 553–556.

- [26] S. Woo, J. Park, J.-Y. Lee, and I. S. Kweon, "Cbam: Convolutional block attention module," in *Proceedings of the European conference on computer vision (ECCV)*, 2018, pp. 3–19.
- [27] O. Petit, N. Thome, C. Rambour, L. Themyr, T. Collins, and L. Soler, "U-net transformer: Self and cross attention for medical image segmentation," in *Machine Learning in Medical Imaging: 12th International Workshop, MLMI 2021, Held in Conjunction with MICCAI 2021, Strasbourg, France, September 27, 2021, Proceedings 12*. Springer, 2021, pp. 267–276.
- [28] G. Xu, X. Zhang, X. He, and X. Wu, "Levit-unet: Make faster encoders with transformer for medical image segmentation," in *Chinese Conference on Pattern Recognition and Computer Vision (PRCV)*. Springer, 2023, pp. 42–53.
- [29] B. Graham, A. El-Nouby, H. Touvron, P. Stock, A. Joulin, H. Jégou, and M. Douze, "Levit: a vision transformer in convnet's clothing for faster inference," in *Proceedings of the IEEE/CVF international conference on computer vision*, 2021, pp. 12 259–12 269.
- [30] A. Hatamizadeh, Y. Tang, V. Nath, D. Yang, A. Myronenko, B. Landman, H. R. Roth, and D. Xu, "Unetr: Transformers for 3d medical image segmentation," in *Proceedings of the IEEE/CVF winter conference on applications of computer vision*, 2022, pp. 574–584.
- [31] A. Shaker, M. Maaz, H. Rasheed, S. Khan, M.-H. Yang, and F. S. Khan, "Unetr++: delving into efficient and accurate 3d medical image segmentation," *arXiv preprint arXiv:2212.04497*, 2022.
- [32] K. Wang, H. S. Tan, and R. Mcbeth, "Swin unetr++: Advancing transformer-based dense dose prediction towards fully automated radiation oncology treatments," *arXiv preprint arXiv:2311.06572*, 2023.
- [33] Z. Liu, Y. Lin, Y. Cao, H. Hu, Y. Wei, Z. Zhang, S. Lin, and B. Guo, "Swin transformer: Hierarchical vision transformer using shifted windows," in *Proceedings of the IEEE/CVF international conference on computer vision*, 2021, pp. 10 012–10 022.
- [34] B. Li, W. Wu, Q. Wang, F. Zhang, J. Xing, and J. Yan, "Siamrpn++: Evolution of siamese visual tracking with very deep networks," in *Proceedings of the IEEE/CVF conference on computer vision and pattern recognition*, 2019, pp. 4282–4291.
- [35] L. Team, "Labelme.ai: The open source labeling tool," 2024, accessed: 2024-05-16. [Online]. Available: <https://github.com/labelmeai>
- [36] F. Milletari, N. Navab, and S.-A. Ahmadi, "V-net: Fully convolutional neural networks for volumetric medical image segmentation," in *2016 fourth international conference on 3D vision (3DV)*. Ieee, 2016, pp. 565–571.